

Antiferromagnetic Hysteresis above the Spin Flop Field

M. J. Grzybowski,^{1,*} C. F. Schippers,¹ O. Gomonay,² K. Rubi,³ M. E. Bal,³ U. Zeitler,³ B. Koopmans,¹ and H. J. M. Swagten¹

¹Department of Applied Physics, Eindhoven University of Technology, PO Box 513, 5600 MB Eindhoven, The Netherlands

²Institute of Physics, Johannes Gutenberg-University Mainz, 55128 Mainz, Germany

³High Field Magnet Laboratory (HFML -EMFL), Radboud University, 6525 ED Nijmegen, The Netherlands

(Dated: September 2, 2021)

Magnetocrystalline anisotropy is essential in the physics of antiferromagnets and commonly treated as a constant, not depending on an external magnetic field. However, we demonstrate that in CoO the anisotropy should necessarily depend on the magnetic field, which is shown by the spin Hall magnetoresistance of the CoO/Pt device. Below the Néel temperature CoO reveals a spin-flop transition at 240 K at 7.0 T, above which a hysteresis in the angular dependence of magnetoresistance unexpectedly persists up to 30 T. It is most likely due to the presence of the unquenched orbital momentum, which can play an important role in antiferromagnetic spintronics.

Antiferromagnetic thin-film materials have attracted a lot of attention recently due to their unique properties that create potential applications in spintronics such as data storage [1, 2] or long-distance spin transport [3, 4]. Their robustness against external magnetic fields is an important promise for using these antiferromagnetic materials. Therefore, they demand strong magnetic fields for reorientation of the spins. Unlike ferromagnetic materials, the understanding of the impact of high magnetic fields is essential in antiferromagnets. The behavior of an antiferromagnet (AF) in high magnetic fields is governed by the competition between magneto-crystalline anisotropy and antiferromagnetic exchange interactions. Detailed knowledge of this anisotropy is key to determine possible magnetic configurations of an antiferromagnet as well as proper device design and experimental geometry for potential applications. It is common and well-documented to treat the anisotropy as a physical parameter that is strictly constant for a given temperature [5–7].

In this letter, we present an experimental study of spin reorientation induced by the strong magnetic fields in CoO with an adjacent Pt layer. When the magnetic field \mathbf{B} is applied to an AF along an easy axis, the Néel vector \mathbf{n} , which is the difference of the two spin sublattice magnetizations, may reorient perpendicularly to the field. It is a well-known spin-flop transition and occurs at the spin-flop field B_{SF} , which depends on the magnetic anisotropy. This reorientation of \mathbf{n} can be detected by the spin Hall magnetoresistance (SMR) [5–9]. The angular dependence of the SMR allows extracting the spin-flop field values for different geometrical configurations of the magnetic field and thus, the intriguing behavior of the anisotropy in CoO can be observed. The spin-flop transition is clearly detected together with a remarkable presence of the hysteretic behavior of the AF that cannot be explained by a constant anisotropy field commonly applied for antiferromagnets. Unexpectedly, hysteresis loops in the angular dependence of magnetoresistance persist up to the highest tested magnetic field equaling 30 T. This can be understood as a magnetic anisotropy that should necessarily depend on the external magnetic field magnitude and orientation.

The electrical measurements were performed on a Hall bar device made of a CoO thin film of 5 nm thickness prepared

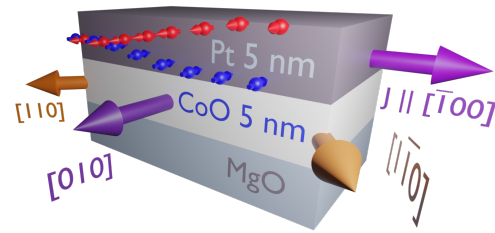


FIG. 1. The scheme of the structure used for the experiments. \mathbf{J} represents the current direction. Magnetic easy (hard) axes are marked by orange (violet) arrows. Blue and red arrows represent the spin accumulation in Pt due to the spin Hall effect.

by means of reactive DC magnetron sputtering on MgO (001) single crystals and capped with 5 nm Pt layer (Fig. 1) [10]. We focus on the analysis of the transverse resistance R_{xy} variations as it can be measured with better accuracy due to the smaller zero-field offset than longitudinal resistance. All data presented in the main text were collected below the Néel temperature at $T = 240$ K. The background signal coming from small sample misalignment with respect to the magnetic field was subtracted [10]. To minimize the contribution of the Pt magnetoresistance into the signal, the subtraction of the resistance variations of the device collected slightly above the T_N at $T = 305$ K was also performed [10].

Initially, the expected in-plane biaxial anisotropy of CoO thin film with easy axes along $[110]$ and $[1\bar{1}0]$ (orange arrows in Fig. 1) is verified [9, 11]. To do this, the in-plane magnetic field of 30 T is applied along the expected easy axis $[1\bar{1}0]$ to set a well-defined AF state of $\mathbf{n} \parallel [110]$. Afterwards, the actual field sweep from 0 to 30 T is performed with the fixed orientation of $\mathbf{B} \parallel [110]$ and the resistance is measured (Fig. 2). Upon increasing the magnitude of \mathbf{B} the signal is initially constant and then an abrupt change of R_{xy} can be seen at $B = 7$ T. This significant change appears only when the magnitude of B is increasing. No relaxation to the initial resistance state is observed within the time scale of the experiment. Similar behavior is observed with the magnetic field pointing along another easy axis (see [10]). The abrupt change of R_{xy} does not appear above the Néel temperature [10]. It does not cor-

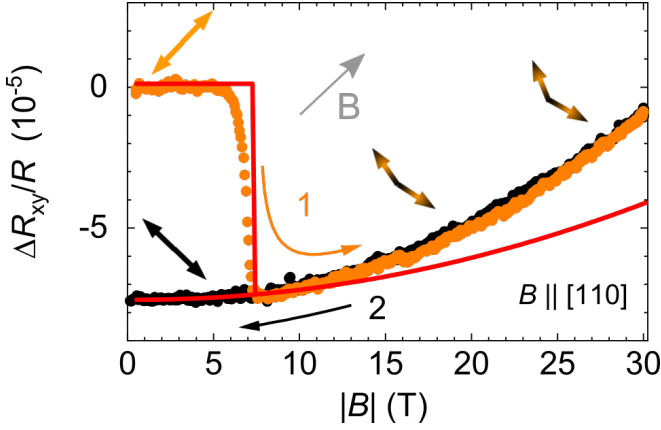


FIG. 2. Transverse magnetoresistance for the CoO structure collected for B along the $[110]$ easy axis. Orange (black) data points correspond to the experiment with increasing (decreasing) magnetic field. The order of the measurements is indicated by the digits. The expected shape of the SMR signal calculated within the macrospin model for $B_{sf} = 7.0$ T is presented by the red curve. The thick arrows represent the directions of the spins (spin canting, angle not to scale) with respect to the magnetic field (thin grey arrow). The electrical signal is expressed as $\Delta R_{xy}/R$, where ΔR_{xy} is the difference in resistance between a data point taken in a magnetic field and the initial value $R_{xy}(B = 0)$. The mean sheet resistance is denoted by R .

relate with any random fluctuations of temperature. Finally, the probing current density does not change during the experiments, so the thermal effects can be ruled out. Therefore, the electrical signal can be attributed to the transverse SMR. The abrupt change of resistance at 7 T reflects the spin-flop transition, where the Néel vector \mathbf{n} changes the orientation from $\mathbf{B} \parallel \mathbf{n}$ to $\mathbf{B} \perp \mathbf{n}$ when B is increasing. The resistance change at the spin flop is consistent with the negative sign of SMR [5, 9, 12]. Nonlinear behavior of SMR in high fields can originate from progressive spin canting and the occurrence of small net magnetic moment \mathbf{m} as depicted symbolically by double-color arrows in Fig. 2.

To verify the qualitative understanding of the obtained results, we construct a macrospin model. Two magnetic moments coupled antiferromagnetically are considered. The energy expression [13] can be formulated as follows:

$$E(\mathbf{n}) = \frac{2}{B_{sf}^2} (\mathbf{B} \cdot \mathbf{n})^2 - (n_x^4 + n_y^4) + \frac{B_{an\parallel}}{B_{an\perp}} n_z^2. \quad (1)$$

In-plane biaxial anisotropy field and out-of-plane uniaxial anisotropy field are represented by $B_{an\perp}$ and $B_{an\parallel}$, respectively. The two orthogonal easy directions in-plane are denoted as x, y and correspond to $[110]$ and $[\bar{1}\bar{1}0]$, respectively (Fig. 1). The spin-flop field is denoted by B_{sf} and equals $B_{sf} = 2\sqrt{B_{ex}B_{an\perp}}$, where B_{ex} is the exchange field. The value of B_{sf} is determined from the experimental data (Fig. 2). \mathbf{B} remains in the plane of the sample in all experiments. The spins are expected to remain in-plane due to thin-film character of the sample [9, 11] and the out-of-plane anisotropy field is set $B_{an\parallel} \gg B_{an\perp}$. We perform the energy minimization with B_{sf}

and coordinates of \mathbf{B} as the only parameters obtaining the expected orientation of \mathbf{n} . With the assumption of $B \ll B_{ex}$, the magnitude of finite \mathbf{m} perpendicular to \mathbf{n} due to the tilt of the spin sublattices can be estimated [10, 13]. The SMR signal can be modeled by $R_{xy} \propto \rho_n n_{\parallel} n_{\perp} + \rho_m m_{\parallel} m_{\perp}$. For qualitative analysis, it is enough to approximate the ratio between ρ_n and ρ_m [10]. We expect that SMR probes the orientation of the spin only, not the orbital angular momentum L since the current density used in the experiment yields an effective magnetic field that does not exceed 0.4 T as calculated based on the current-field equivalence [9]. Such low fields are not the region where effects coming from unquenched L are observed unlike for the high magnetic field regime as will be discussed below.

Comparison of the model to the field sweep along $[110]$ presented in Fig. 2 reveals good agreement. The modeled SMR marked as a red line exhibits the same qualitative behavior as the measurements. It confirms that the sample exposed previously to the $B \parallel [\bar{1}\bar{1}0]$ and $B \gg B_{sf}$ can be well described by a single domain model. The model also reproduces the quadratic dependence (red solid line in Fig. 2) of the SMR that can be due to spin canting in high fields. The quantitative discrepancy between the model and the experiment in high fields originates most likely from a residual magnetoresistive behavior of Pt that could not be fully subtracted due to its temperature dependence.

Despite a good correlation between the model and the experimental data for the field along an easy direction, we find that the model cannot describe the measurements for the magnetic field along a hard axis [10]. To clarify it, we perform an angular dependence of magnetoresistance (ADMIR) measurements at different magnetic fields and show the data for $B = 10$ T and $B = 25$ T in Fig. 3 and in Fig. 4, respectively. These angle-dependent measurements determine how \mathbf{n} evolves upon gradually changing the magnetic field direction from an easy to a hard axis and consequently conclude about the \mathbf{n} state in the latter case. In ADMIR, the magnetic field vector has a fixed magnitude but it rotates with respect to the crystalline axes. The resistance is recorded as a function of an angle α that the magnetic field forms with $[010]$, which is a hard axis. Above the $B_{sf} = 7$ T, \mathbf{n} is expected to follow the direction perpendicular to \mathbf{B} , which is high enough to overcome the in-plane anisotropy [7]. This should be reflected in the SMR signal that is shown by the red dotted lines in Fig. 3 and in Fig. 4, which is the result of the macrospin model calculation with experimentally determined B_{sf} .

Remarkably, the experiments show a completely different SMR dependence. When the magnetic field changes the orientation from $\alpha = 90^\circ$ to $\alpha = -90^\circ$ and back the electrical signal follows the same trend except for the region close to $\alpha = 0^\circ$. In the vicinity of $\alpha = 0^\circ$, the point where the magnetic field points along the hard axis, the SMR shows a hysteresis loop (Fig. 3 and Fig. 4). At higher magnetic fields the hysteresis becomes narrower. The hysteresis can be characterized by its width and plotted as a function of \mathbf{B} (Fig. 5). Then, it can be clearly seen that hysteresis loops appear in

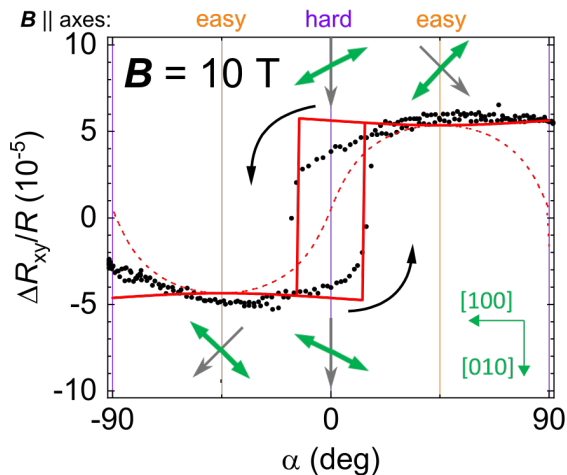


FIG. 3. The angular dependence of magnetoresistance for the CoO structure collected at $B = 10$ T is depicted by the black dots. It is expressed as relative changes of the resistance as a function of an angle α that \mathbf{B} forms with the [010] crystalline direction. Green (grey) arrows represent the spin (magnetic field) orientation with respect to crystalline axes (coordinates in bottom right corner). Black arrows depict the angle sweeping direction. The dotted red line displays modeled behavior of the ADRM with $B_{sf} = 7$ T. Introduction of the new energy term into the model with $\xi = -0.082$ can reproduce the hysteresis as illustrated by the red continuous curve.

the whole range of tested magnetic fields between B_{sf} up to 30 T. The hysteresis loops are absent above T_N and they can be attributed to the antiferromagnetic behavior of CoO. Below B_{sf} , no abrupt resistance changes are detectable and only slight residual hysteretic behavior around $\alpha = 0$ can be observed that can be due to possible domain structure in the system. The ADMR measurements reveal that for $\mathbf{B} \parallel [010]$ and $B > B_{sf}$ different states of the AF are possible depending on the history and the system behaves as if it is always below the spin-flop field. The experimental results can be understood as the Néel vector lagging behind the magnetic field due to the strong in-plane anisotropy. However, such effect is expected only below B_{sf} , but should be absent above the spin-flop field in our current understanding of the interplay between Zeeman energy, antiferromagnetic exchange, and anisotropy energy, where \mathbf{n} should follow the direction perpendicular to the magnetic field [7].

In order to interpret the experimental data, we assume that the magnetic field modifies the magnetic anisotropy of the antiferromagnet. We describe this contribution by introducing an additional energy term:

$$E_a = \xi B_x B_y n_x n_y \quad (2)$$

into the equation (1). It appears only if the magnetic field has nonzero components for both easy directions. Thus, it follows the symmetry of the experimental observations and can describe the unexpected hysteretic behavior of the antiferromagnet when a strong magnetic field is parallel to a hard

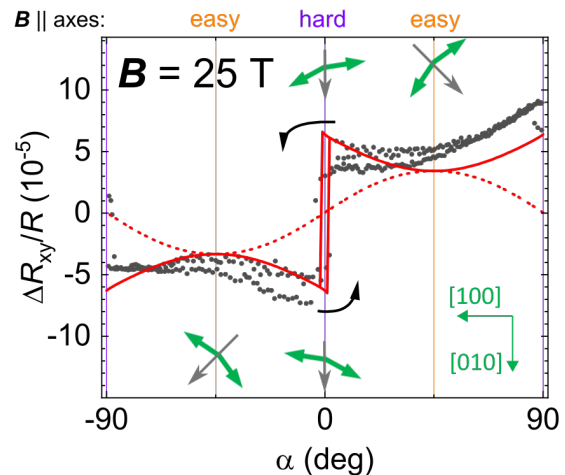


FIG. 4. The angular dependence of the magnetoresistance for $B = 25$ T. Experimental results (black points) are compared to the macrospin models with $\xi = 0$ (red dotted line) and $\xi = -0.082$ (red continuous curve). The corresponding spins (magnetic field) orientation with respect to the crystalline axes with the coordinates in bottom right corner are symbolized by the thick green (grey) arrows.

direction. For negative ξ such contribution enhances the energy barrier separating between the states with different orientations of the Néel vector seen as an enhancement of the effective anisotropy field. We believe that this contribution originates from the field-induced tilting of the orbital momentum from the easy axis.

The existence of the hysteresis loop in SMR can be reproduced by the new model with $\xi = -0.082$ as demonstrated by the solid red lines in Fig. 3 and Fig. 4. Good agreement of the hysteresis width between the model and experiments is obtained for all magnetic fields tested experimentally (Fig. 5). Slight deviations from the model that can be seen in the experimental data in Fig. 3 as a rounded shape of the hysteresis loop and a difference in the curvature near $\alpha = \pm 45^\circ$ can be interpreted as a sign of a domain structure and magnetic inhomogeneity of the system. For the model with $\xi = 0$, which corresponds to the original equation (1) and constant magnetic anisotropy, no hysteresis above the B_{sf} is expected as indicated by red dotted line in Fig. 3 and 4 as well as green circles in Fig. 5.

A likely explanation for the observed hysteretic behavior and the additional energy term $\xi B_x B_y n_x n_y$ is the unquenched orbital momentum that is known to be present in CoO and has a strong contribution to the magnetocrystalline anisotropy in this material [14, 15]. It has also been observed to manifest itself in the magnon spectrum [16]. We restrict our discussion to the simplest case to qualitatively justify the orbital momentum dependence on the magnetic field and its influence on the anisotropy. First, we note that spin-orbit coupling induces an antiparallel alignment of the effective $L = 1$ orbital momenta \mathbf{L}_1 and \mathbf{L}_2 to the corresponding magnetic spins for each of sublattices [16]. The external magnetic field $B \leq B_{sf}$

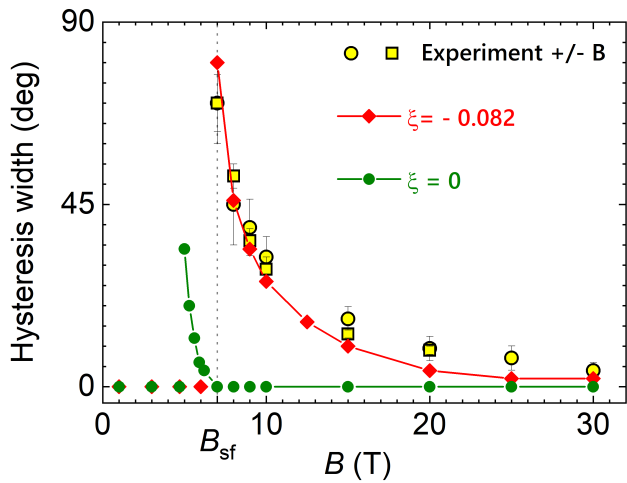


FIG. 5. Summary of the hysteresis width observed in ADMR as a function of the magnetic field (yellow squares and circles). The macrospin model with $\xi = 0$ (green circles) predicts the occurrence of a hysteresis only slightly below B_{sf} , whereas setting $\xi = -0.082$ (red diamonds) yields good agreement with the measurements. Lines are guides for the eye.

aligned parallel to the magnetic spins does not change this configuration; the orbital angular momenta are quenched in the lowest states with $|L_{1,2x}| = 1$ (where the quantization axis x is parallel to the easy axis). However, the magnetic field, oriented generically in the xy -plane, induces mixing of the states with the projections $L_{jx} = \pm 1$, and 0. This mixing, in turn, results in a nonzero expectation values of quadrupolar variables, $\langle \hat{L}_{jx} \hat{L}_{jy} \rangle$ ($j = 1, 2$) and additional spin anisotropy $K_{an}^{ha} A_{xy}(\mathbf{B}) n_x n_y$ with $A_{xy}(\mathbf{B}) = \sum_{j=1,2} \langle \hat{L}_{jx} \hat{L}_{jy} \rangle$.

To calculate the quantum states of the orbital momenta we introduce the hamiltonian

$$\hat{\mathcal{H}} = \sum_{j=1,2} \left[-K^L (\hat{\mathbf{L}}_j \mathbf{e}_j)^2 + \lambda \mathbf{S}_j \hat{\mathbf{L}}_j + 2\mu_B \mathbf{B} \hat{\mathbf{L}}_j \right], \quad (3)$$

where K^L is anisotropy of the angular momentum, the constant λ parametrizes spin-orbit coupling, μ_B is the Bohr magneton. We assume that the orientation of the Néel vectors is fixed along x and the local quantization axes \mathbf{e}_j are parallel/antiparallel to the Néel vector ($\mathbf{e}_1 \uparrow \downarrow \mathbf{e}_2 \uparrow \uparrow \hat{x}$).

Figure 6 shows the field dependence of $A_{xy}(\mathbf{B})$ (see supplementary material for more details). Below the critical field (red line) $A_{xy}(\mathbf{B})$ is close to zero, as the quadrupoles $\langle \hat{L}_{1x} \hat{L}_{1y} \rangle$ and $\langle \hat{L}_{2x} \hat{L}_{2y} \rangle$ have opposite signs and almost compensate each other. However, close to the critical field value, the magnetic field is large enough to align both orbital momenta parallel to the magnetic field, and both quadrupoles have the same sign. This induces a rapid increase of $A_{xy}(\mathbf{B})$ above the critical field with the maximum anisotropy value achieved for the field parallel to the hard axis. There is a nonlinear dependence of $A_{xy}(\mathbf{B})$ on the magnetic field [10] above the critical field which we substitute with the B^2 relation for simplicity in our phenomenological energy term (equation 2). The value of

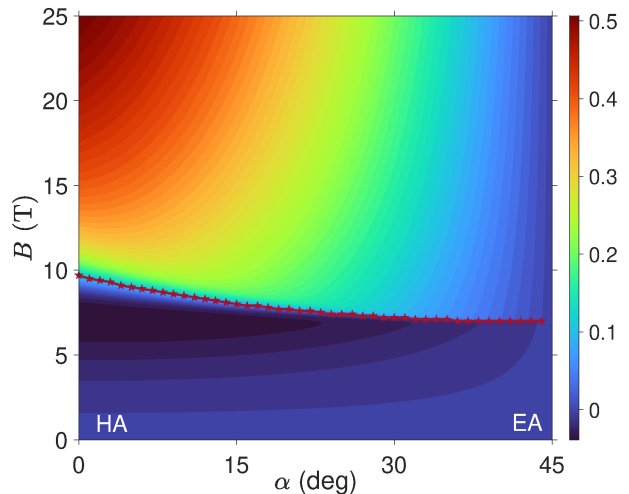


FIG. 6. The value of the field-induced anisotropy $A_{xy}(\mathbf{B}) \equiv \sum_{j=1,2} \langle \hat{L}_{jx} \hat{L}_{jy} \rangle$ (color code, dimensionless) as a function of the orientation and the magnitude of the magnetic field. The star line shows the value of the threshold field $B_{thresh}(\alpha)$ below which the anisotropy is negligible. The HA and EA denote a hard and an easy axis, respectively.

the critical field scales with spin-orbit coupling λ and corresponds to the spin-flop field B_{sf} if \mathbf{B} is parallel to an easy axis. We conjecture that a direct experimental confirmation of such behavior of the angular momentum could be performed, for example, by studying the magnetic field induced frequency shift of the magnon modes with optical excitation.

To summarize, we report the observation of the hysteresis loops in the angular dependence of magnetoresistance of a thin film of CoO with adjacent Pt. The hysteretic behavior is unexpectedly present above the spin-flop field and persists up to the highest tested magnetic fields (30T). It can be interpreted by the dependence of the magnetic anisotropy on the external magnetic field. The unquenched orbital angular momentum is a likely reason for the observed effects. These findings highlight the role of the anisotropy variations induced by the magnetic field and the role of the unquenched orbital momentum in the physics of antiferromagnets and their potential applications. The anisotropy dependence on the magnetic field may modify the expected equilibrium spin state of antiferromagnets in electrical experiments that strongly rely on the generation of the effective magnetic field.

We would like to thank Rembert Duine, Reinoud Lavrijsen, Marta Gryglas-Borysiewicz and Tomasz Dietl for helpful discussions. We acknowledge Pim Lueb for VSM-SQUID measurements. We acknowledge support from HFML-RU, member of the European Magnetic Field Laboratory (EMFL). Sample fabrication was performed using NanoLabNL facilities. The research was funded by the Dutch Research Council (NWO) under Grant 680-91-113. O.G. acknowledges support from the Alexander von Humboldt Foundation, the ERC Synergy Grant SC2 (No. 610115), and the Deutsche Forschungs-

gemeinschaft (DFG, German Research Foundation) - TRR 173 – 268565370 (project B12).

* m.j.grzybowski@tue.nl

- [1] P. Wadley, B. Howells, J. Zelezny, C. Andrews, V. Hills, R. P. Campion, V. Novak, K. Olejnik, F. Maccherozzi, S. S. Dhesi, S. Y. Martin, T. Wagner, J. Wunderlich, F. Freimuth, Y. Mokrousov, J. Kune, J. S. Chauhan, M. J. Grzybowski, A. W. Rushforth, K. W. Edmonds, B. L. Gallagher, and T. Jungwirth, Electrical switching of an antiferromagnet, *Science* **351**, 587 (2016).
- [2] T. Jungwirth, X. Marti, P. Wadley, and J. Wunderlich, Antiferromagnetic spintronics, *Nature Nanotechnology* **11**, 231 (2016).
- [3] R. Lebrun, A. Ross, S. A. Bender, A. Qaiumzadeh, L. Baldrati, J. Cramer, A. Brataas, R. A. Duine, and M. Kläui, Tunable long-distance spin transport in a crystalline antiferromagnetic iron oxide, *Nature* **561**, 222 (2018).
- [4] J. Han, P. Zhang, Z. Bi, Y. Fan, T. S. Safi, J. Xiang, J. Finley, L. Fu, R. Cheng, and L. Liu, Birefringence-like spin transport via linearly polarized antiferromagnetic magnons, *Nature Nanotechnology* **15**, 563 (2020).
- [5] G. R. Hoogeboom, A. Aqeel, T. Kuschel, T. T. M. Palstra, and B. J. van Wees, Negative spin Hall magnetoresistance of Pt on the bulk easy-plane antiferromagnet NiO, *Applied Physics Letters* **111**, 052409 (2017).
- [6] L. Baldrati, A. Ross, T. Niizeki, C. Schneider, R. Ramos, J. Cramer, O. Gomonay, M. Filianina, T. Savchenko, D. Heinze, A. Kleibert, E. Saitoh, J. Sinova, and M. Kläui, Full angular dependence of the spin Hall and ordinary magnetoresistance in epitaxial antiferromagnetic NiO(001)/Pt thin films, *Physical Review B* **98**, 024422 (2018).
- [7] S. Geprägs, M. Opel, J. Fischer, O. Gomonay, P. Schwenke, M. Althammer, H. Huebl, and R. Gross, Spin Hall magnetoresistance in antiferromagnetic insulators, *Journal of Applied Physics* **127**, 243902 (2020).
- [8] J. Fischer, O. Gomonay, R. Schlitz, K. Ganzhorn, N. Vlietstra, M. Althammer, H. Huebl, M. Opel, R. Gross, S. T. B. Goennenwein, and S. Geprägs, Spin Hall magnetoresistance in antiferromagnet/heavy-metal heterostructures, *Physical Review B* **97**, 014417 (2018).
- [9] L. Baldrati, C. Schmitt, O. Gomonay, R. Lebrun, R. Ramos, E. Saitoh, J. Sinova, and M. Kläui, Efficient Spin Torques in Antiferromagnetic CoO/Pt Quantified by Comparing Field-And Current-Induced Switching, *Physical Review Letters* **125**, 77201 (2020).
- [10] Supplementary Material.
- [11] W. N. Cao, J. Li, G. Chen, J. Zhu, C. R. Hu, and Y. Z. Wu, Temperature-dependent magnetic anisotropies in epitaxial Fe/CoO/MgO(001) system studied by the planar Hall effect, *Applied Physics Letters* **98**, 262506 (2011).
- [12] H. Nakayama, M. Althammer, Y.-T. Chen, K. Uchida, Y. Kajiwara, D. Kikuchi, T. Ohtani, S. Geprägs, M. Opel, S. Takahashi, R. Gross, G. E. W. Bauer, S. T. B. Goennenwein, and E. Saitoh, Spin Hall Magnetoresistance Induced by a Nonequilibrium Proximity Effect, *Physical Review Letters* **110**, 206601 (2013).
- [13] H. V. Gomonay and V. M. Loktev, Spin transfer and current-induced switching in antiferromagnets, *Physical Review B* **81**, 144427 (2010).
- [14] J. Kanamori, Theory of the Magnetic Properties of Ferrous and Cobaltous Oxides, I, *Progress of Theoretical Physics* **17**, 177 (1957).
- [15] J. Kanamori, Theory of the Magnetic Properties of Ferrous and Cobaltous Oxides, II, *Progress of Theoretical Physics* **17**, 197 (1957).
- [16] T. Satoh, R. Iida, T. Higuchi, Y. Fujii, A. Koreeda, H. Ueda, T. Shimura, K. Kuroda, V. I. Butrim, and B. A. Ivanov, Excitation of coupled spin-orbit dynamics in cobalt oxide by femtosecond laser pulses, *Nature Communications* **8**, 638 (2017).
- [17] N. Vlietstra, J. Shan, V. Castel, B. J. van Wees, and J. Ben Youssef, Spin-Hall magnetoresistance in platinum on yttrium iron garnet: Dependence on platinum thickness and in-plane/out-of-plane magnetization, *Physical Review B* **87**, 184421 (2013).
- [18] J. H. Han, C. Song, F. Li, Y. Y. Wang, G. Y. Wang, Q. H. Yang, and F. Pan, Antiferromagnet-controlled spin current transport in SrMnO₃/Pt hybrids, *Physical Review B* **90**, 144431 (2014).
- [19] G. A. Carson, M. H. Nassir, and M. A. Langell, Epitaxial growth of Co₃O₄ on CoO(100), *Journal of Vacuum Science & Technology A: Vacuum, Surfaces, and Films* **14**, 1637 (1996).
- [20] Y. Li, W. Qiu, F. Qin, H. Fang, V. G. Hadjiev, D. Litvinov, and J. Bao, Identification of Cobalt Oxides with Raman Scattering and Fourier Transform Infrared Spectroscopy, *The Journal of Physical Chemistry C* **120**, 4511 (2016).
- [21] R. Hayes and C. Perry, Magnetic excitations in cobalt oxide, *Solid State Communications* **14**, 173 (1974).
- [22] S. Vélez, V. N. Golovach, A. Bedoya-Pinto, M. Isasa, E. Sagasta, M. Abadia, C. Rogero, L. E. Hueso, F. S. Bergeret, and F. Casanova, Hanle Magnetoresistance in Thin Metal Films with Strong Spin-Orbit Coupling, *Physical Review Letters* **116**, 016603 (2016).